Check for updates

Spatio-temporal changes and hydrological forces of wetland landscape pattern in the Yellow River Delta during 1986–2022

Mengqi Qiu · Yanxu Liu · Peng Chen · Naijie He · Shuai Wang · Xinzi Huang · Bojie Fu

Abstract

Context Estuarine wetlands provide valuable ecosystem services, but 20–78% of coastal wetlands are facing the risk of loss by the end of the century. The Yellow River Delta (YRD) wetland, one of the most productive delta areas in the world, has undergone dramatic changes under the influence of a precipitous drop of sediment delivery and runoff, coupled with the invasion of *Spartina alterniflora*. Monitoring the spatio-temporal patterns, thresholds, and drivers of change in wetland landscapes is critical for sustainable management of delta wetlands.

Objectives Generate annual mapping of salt marsh vegetation in the YRD wetland from 1986 to 2022, analyze the trends of wetland patch area and landscape pattern, and explain the hydrological drivers of landscape pattern evolution.

Methods We combined Landsat 5−8 and Sentinel-2 images, vegetation phenology, remote sensing indices, and Random Forest supervised classification to map the typical salt marsh vegetation of the YRD. We applied piecewise linear regression to analyze YRD wetland changes and stepwise multiple linear regression to assess the impact of hydrological factors on landscape pattern.

Results We identified three stages of landscape pattern evolution with 1997 and 2009 as critical junctures, including the rapid expansion stage, gradual decline stage, and bio-invasion stage. In the rapid expansion stage, the wetland area expanded by 70%, while the typical salt marsh vegetation (*Phragmites australis*) area was reduced by 25%. In the gradual decline stage, the wetland was reduced by 21% and the *Phragmites australis* area was reduced by 16%. In the bio-invasion stage, coverage of *Spartina alterniflora* expanded rapidly, with a 68-fold increase in area

M. Qiu · Y. Liu (✉) · P. Chen · S. Wang
State Key Laboratory of Earth Surface Processes
and Resource Ecology, Faculty of Geographical Science,
Beijing Normal University, Xinjiekouwai Street No. 19,
Haidian District, Beijing 100857, China
e-mail: yanxuliu@bnu.edu.cn

M. Qiu
e-mail: qiuqiu@mail.bnu.edu.cn

N. He
School of Mathematical Sciences, Soochow University,
Shizi Street No. 1, Gusu District, Suzhou 215006, Jiangsu,
China

X. Huang
Beijing No.4 High School International Campus, No.2
Zongmaotoutiao, Xitiejianghutong, Beijing 100031, China

B. Fu
State Key Laboratory of Urban and Regional Ecology,
Research Center for Eco-Environmental Sciences, Chinese
Academy of Sciences, Shuangqing Road No. 18, Haidian
District, Beijing 100085, China
e-mail: bfu@rcees.ac.cn

relative to 2009, expanding at an average rate of 344 hm^2 per year.

Conclusions Areas of total wetland, tidal flat, and *Phragmites australis* were significantly influenced by cumulative sediment delivery and cumulative runoff, which together explained 61.5%, 75.7% and 63.8% of their variation, respectively. Wetland and tidal flat areas increased with cumulative sediment delivery, while cumulative runoff had a weak negative effect. For *Phragmites australis*, cumulative runoff had a positive effect, whereas cumulative sediment delivery had a negative effect. Water resources regulation measures should be taken to prevent the degradation of wetland ecosystems, and intervention measures can be implemented during the seedling stage to control the invasion of *Spartina alterniflora*.

Keywords Salt marsh vegetation · Time series · Vegetation classification · Hydrologic drivers · Landscape indices

Introduction

Estuarine deltas present a global hotspot for ecological conservation and socio-economic development (Nienhuis et al. 2020; Reader et al. 2022). These deltas, characterized by fertile arable land, integrated transport nodes driving modern industry, and bountiful aquatic resources sustaining human populations, stand as the cradle of human civilization (Loucks 2019; Chen and Kirwan 2022; Törnqvist 2023). Although they cover a mere 0.56% of the Earth's surface, estuarine deltas house 4.1% of the global population, with more than 339 million people living there (Edmonds et al. 2020). Wetlands in the estuarine deltas have unique coastal ecosystems that provide a wide range of ecological services, including climatic regulation, carbon sequestration and biodiversity conservation (Xia et al. 2020; Reid 2005; Liu et al. 2023a, b; Yin et al. 2023). Unfortunately, estuarine wetlands are dynamic, sensitive and vulnerable systems (Ward et al. 2020), which are easily disturbed by environmental changes (e.g. flood, saltwater intrusion, sea level rise and biological invasion) (Barbier 2014; Cox et al. 2022; Zhang et al. 2023), coupled with anthropogenic pressures (e.g. agricultural expansion, urbanization and water resource development) (Murray et al. 2022; Lin and Yu 2018; Fu et al. 2022;

Ye et al. 2020). In such a complicated and volatile environment, estuarine wetlands are facing serious risks of area loss and ecological degradation (Li et al. 2022a, b; Gong et al. 2023; Liu et al. 2023a, b). It is estimated that 20–78% of coastal wetlands will be lost under high sea-level rise accompanied by maximum dike construction by the end of the century, resulting in a profound erosion of biodiversity and an increased risk of flooding (Spencer et al. 2016; Rodríguez et al. 2017). Therefore, precise monitoring of the dynamic spatio-temporal patterns within wetland landscapes is critical for effective conservation, restoration and sustainable management of delta wetlands.

Recent studies on estuarine wetlands primarily focus on area gains and losses driven by human activities and natural processes (Nienhuis et al. 2020; Wang et al. 2020; Osland et al. 2022; Edmonds et al. 2023), or geomorphic changes, especially under hydrodynamics and morphodynamics (Montaño and Carbajal 2008; Paszkowski et al. 2021), as well as ecosystem services assessment (Rosentreter et al. 2023). Murray et al. (2022) used Landsat images to assess changes in the global tidal wetlands over the past two decades and found that over 13,000 km^2 of tidal wetlands have recently been lost, but these losses have mostly been offset by the formation of new wetlands. Lin and Yu (2018) interpreted coastal wetland distribution maps of three coastal city clusters in China. They found that ecological degradation from land conversion due to urbanization caused serious temporal loss of the remaining natural coastal wetlands. However, the lack of detailed time series information hinders the accurate identification of regime shifts in estuarine wetland evolution and increases the uncertainty of identifying driving factors (Wang et al. 2021a). The Sentinel-2 dataset, with its significant advantages in terms of resolution (up to 10m), enables the possibility of long-term and high spatiotemporal resolution wetland mapping (Chang et al. 2022; Zhou 2022; Dong et al. 2016), which can improve our understanding of the multiple hydrological forces that cause regime shifts in estuarine wetland evolution (Murray et al. 2019; Goldberg et al. 2020).

China's Yellow River is the most sediment-filled river on Earth (Wang et al. 2007; Song et al. 2020). Exceptional sediment loads bring excellent land-building function to the Yellow River Delta (YRD) wetland, thus it is considered to have one of the highest ecological conservation values among the river

deltas in China (Cong et al. 2019). Although YRD wetland was designated as a national nature reserve in 1992, listed in the Ramsar Convention on Wetlands in 2013, and approved for the construction of the Yellow River Delta National Park in 2021, the intensification of anthropogenic pressure and the growing impacts of environmental change are still continually affecting its tidal wetlands and component intertidal ecosystems (Zhang et al. 2021a, b; Li et al. 2023). Vegetation of estuary wetlands plays a key role in stabilizing the coast and accreting sediment to mitigate the negative impact of sea level rise (Pang et al. 2023). Salt marsh vegetation in the YRD wetland has changed rapidly. Coupled with the rapid invasion of *Spartina alterniflora* (SA*)* in recent years, the degeneration of native plant populations such as *Phragmites australis* (PA), which dominates wetland biodiversity and carbon sink capacity, has led to a sharp decline in the populations of rare waterfowls that live in habitats containing PA, and thus, the biodiversity of these wetlands is seriously threatened (Zhang et al. 2021a, b). Current monitoring of YRD wetlands mainly focuses on artificial and natural wetlands (Li et al. 2023; Zhan et al. 2023) or single ecosystem types such as woodland or grassland (Chen et al. 2016; Li et al. 2023). Given the difficulty in distinguishing salt marsh vegetation from remote sensing images, not only monitoring of composite ecosystems is inadequate, long-term and continuous interpretation is also scarce (Cong et al. 2019; Li et al. 2023). Moreover, significant changes have taken place in the Yellow River's runoff (RU) and sediment delivery (SE) in the past 60 years (Wang et al. 2016; Song et al. 2020), which will have an important impact on the estuary wetland landscape pattern change and could lead to a regime shift. Therefore, the understanding of the interactions between various hydrological factors and vegetation-type succession in wetland landscapes and ecosystems, as well as the impacts of these multiple driving factors on wetland evolution in the YRD, needs to be updated.

In order to explore the evolution trend of wetland landscape pattern in the YRD and its hydrological driving factors, the objectives of this study are as follows: (1) generate a complete time series mapping of salt marsh vegetation in the YRD from 1986 to 2022 by employing a Random Forest supervised classification method, using Landsat-5/7/8 and Sentinel-2 satellite datasets, (2) analyze the trends of wetland patch area and landscape pattern, and (3) explain the hydrological drivers of landscape pattern evolution in the YRD wetland by exploring the potential associations of wetland patch areas and landscape indices with hydrological factors (such as RU, SE, cumulative runoff (RU+) and cumulative sediment delivery (SE+)).

Methods

Study area

The YRD wetland is located at the mouth of the Yellow River in Dongying City, Shandong Province, facing the Bohai Sag to the east and the West Pacific to the west, backing to the Eurasian continent, between 37°61′- 37°89′N and 119°06′- 119°40′E, with an area of 883.26 km^2, and an average elevation is about 2–10 m (Fig. 1a, b). Since the Yellow River formed, it has undergone 26 major channel shifts (Fig. 1a). Our study area is the modern estuary that stabilized after 1976 and was modified by a manual diversion in 1996. In the 1990s, under the influence of climate drought and human excessive water extraction, temporary periods with no flow occurred frequently on the lower Yellow River, with the longest interval occurring in 1997 (lasted about 226 days) (Kong et al. 2015). Meanwhile, the completion of the Xiaolangdi Dam in 2001, driven by a new regulatory framework, helped stabilize the runoff and sediment delivery. In the recent decades, it has gradually formed one of the world's fastest-growing deltas, representing typical newly formed estuarine wetlands worldwide (Li et al. 2009).

Influenced by soil salinity gradients, the vegetation composition across the YRD wetland has a distinct zonal distribution, with SA, *Suaeda salsa*, and PA occupying sequential niches from the coast to the inland regions (Feng et al. 2018). PA, a dominant freshwater species, mainly thrives in wetland water bodies and along the Yellow River banks (Fig. 1 c2–c4). It serves as vital habitat for rare and endangered bird species, playing a critical role in biodiversity preservation and ecological integrity (Zhang et al. 2021a, b). In contrast, SA is a typical halophytic plant, which primarily flourishes within intertidal zones along the coastal periphery and tidal flats (Wan et al. 2009) (Fig. 1 c2–c4). SA was once considered a
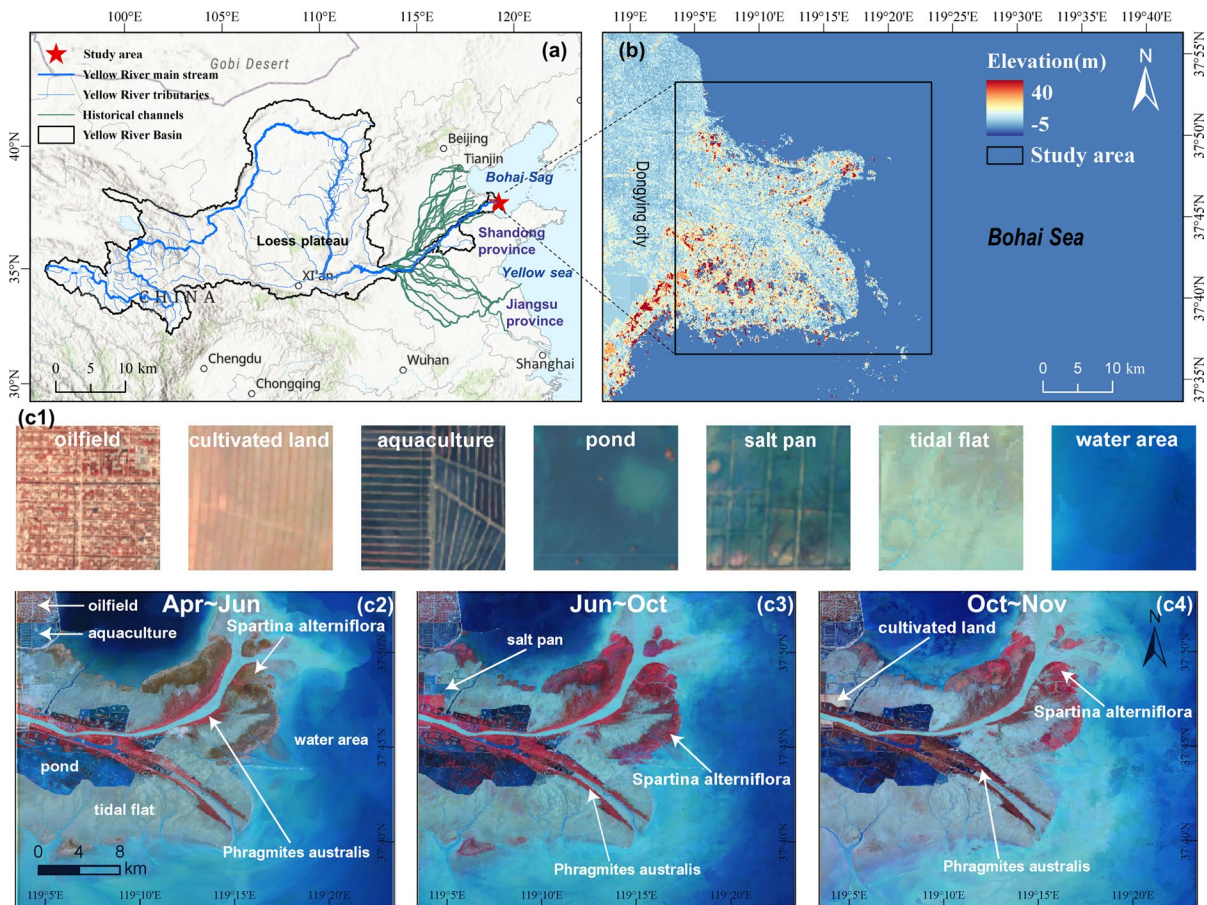
Fig. 1 Location (**a**), elevation (**b**) of the YRD (Yellow River Delta) wetland and interpretive markers of wetland patches in the YRD wetland (c1–c4)

"beach protector" due to its ability to stabilize shores, promote sediment deposition, resist typhoons, and reduce wave impact (Sun et al. 2023). However, propelled by its robust salt tolerance, flood tolerance, and reproductive capacity, it has rapidly spread along the Chinese coastal zone, posing a significant threat to biodiversity (Chang et al. 2022; Huang et al. 2022).

Datasets

Image data and processing

A total of 1728 surface reflectance images over the period 1986–2022 were selected from Landsat-5 TM, Landsat-7 ETM+, and Landsat-8 OLI (the scene of 121/34) imagery with a spatial resolution of 30m and Sentinel-2 MSI (scenes of 50SPG and 50SQG)

imagery with a spatial resolution of 10m and 20m, which are all available from the Google Earth Engine (GEE) cloud computing platform. For the Landsat series datasets, we adopted the Level 2, Collection 2, and Tier 1 versions, which have been subject to systematic radiometric and geometric correction by the United States Geological Survey (Google 2023a). The Sentinel-2 MSI Level-2A imagery not only reduces the impact of atmospheric interference on the spectral measurements, but also includes cloud and atmospheric masks, exhibiting excellent performance in quantitative analysis of the surface landscape (Google 2023b). The number of Landsat images varies by season and year (Fig. 2 a1, a2), averaging 17 images annually. In contrast, the annual average for Sentinel-2 imagery is much higher, at 294 images. Finally, we used the median composite of all images for each
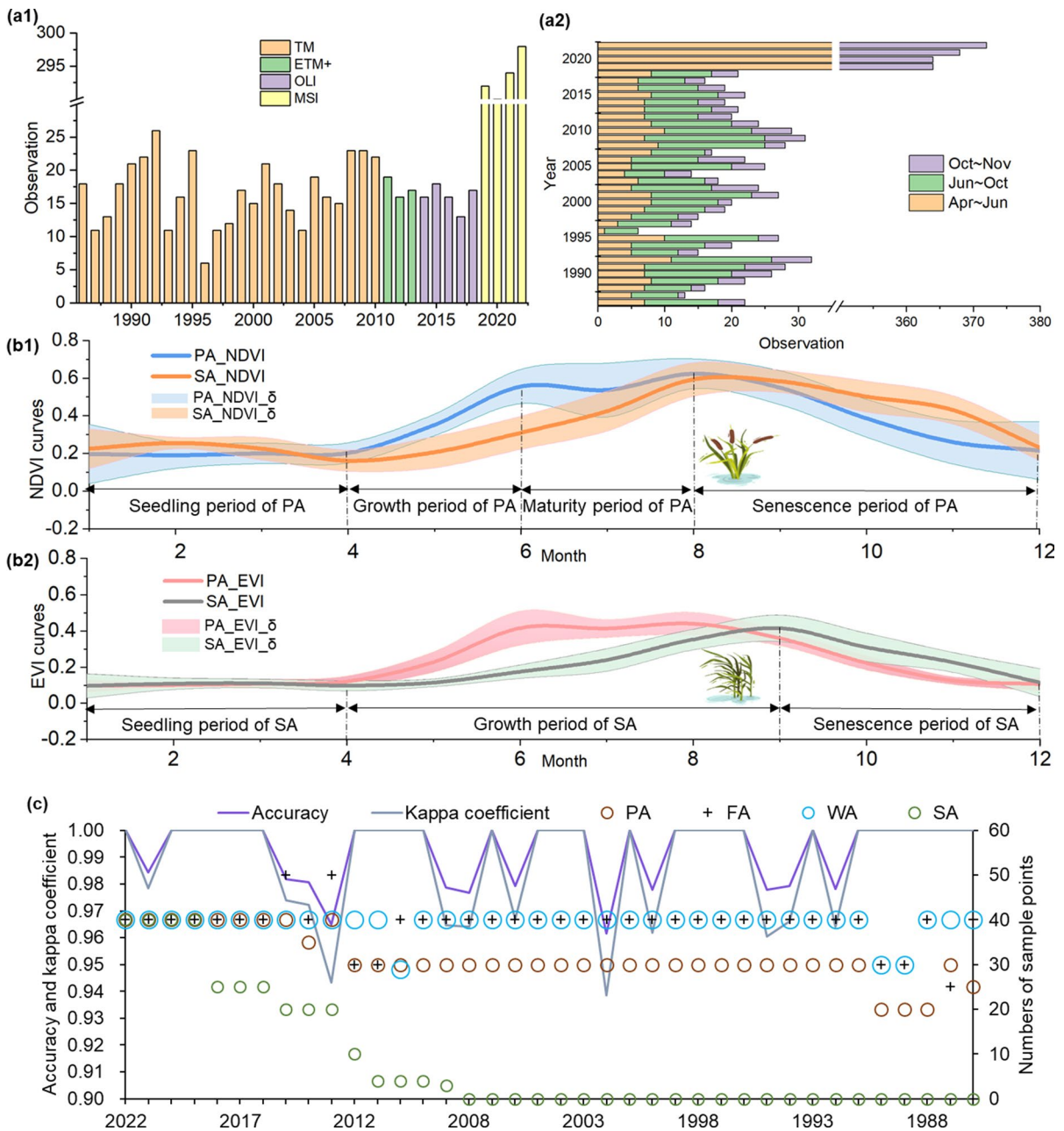
Fig. 2 Available Landsat and Sentinel observation numbers for different sensors and periods during 1986–2022 (a1-a2), NDVI/EVI curves and standard deviation of PA and SA (b1-b2), number of different samples, accuracy and Kappa coefficient of supervised classification (**c**). (b1-b2) The solid line is the mean value of NDVI/EVI during 2011–2021, and the semi-transparent band represents the total standard deviation (δ). The dotted line divides the life cycle of the PA/SA. PA, SA, TA, and WA represent *Phragmites australis, Spartina alterniflora*, tidal flat and water body, respectively

phenological period as the image data for supervised classification.

Hydrological data

Hydrological data were sourced from the hydrological monitoring station located at Lijin, which is

situated in the lowest downstream region of the Yellow River Basin. Specifically, we obtained the annual runoff and sediment delivery data from 1986 to 2021 for the Lijin hydrometric station, which were acquired from the Yellow River Conservancy Commission of the Ministry of Water Resources.

Classification and Assessment

The YRD wetland was classified into four land cover types: water body, tidal flat, PA, and SA. Later, based on field surveys and visual interpretation, additional land cover types such as oilfield, pond, aquaculture, salt pan, and cultivated land were included. The detailed process for monitoring classification is described below.

Phenology identification

PA and SA share remarkable morphological and color similarities, which create significant challenges for accurate cross-temporal supervised classification (Chang et al. 2022). However, there exist discernible differences in the phenology of these saltmarshes, providing an opportunity for differentiation. Both the Normalized Difference Vegetation Index (NDVI) and Enhanced Vegetation Index (EVI) serve as widely used indices for precise vegetation monitoring (Bolton and Friedl 2013; Shammi and Meng 2021). Consequently, we constructed monthly NDVI and EVI time series curves spanning a decade (2011–2021) to elucidate the phenological characteristics of these two saltmarshes.

Prior studies indicate that PA's growth spans April to October, peaking between late July and early August, whereas SA's growth lags behind PA in the YRD wetland by about a month (Zhang et al. 2021a, b; Chang et al. 2022). Therefore, we synthesized remote sensing imagery for three timeframes in 2021: April to June, June to October, and October to November, and displayed in a false-color composite of near-infrared, infrared, and green bands (Fig. 1 c2–c4). These composites revealed distinct color variations for PA and SA throughout these periods: (1) From April to June, PA displayed a bright red shade, while SA exhibited a brownish hue. (2) From June to October, SA's color gradually shifted to a deeper red tone, surpassing the intensity of red in PA and becoming a dark red color. (3) From October to November, PA's color faded,

transitioning to a reddish-brown shade, whereas SA appeared as a bright red color. Subsequently, we incorporated PA and SA samples into the GEE platform for the 2011–2021 period, with varying sample numbers across different years (Fig. 2c). Ultimately, monthly NDVI and EVI time series curves were generated for PA and SA (Fig. 2 b1–b2).

The phenological cycle of PA includes four stages: seedling, growth, maturity, and senescence (Fig. 2 b1). PA experiences vigorous growth from April to June, evident in rising NDVI and EVI curves. From June to August, PA's vegetation follows a bimodal pattern, reaching its annual peak, the maturity stage. Post-August, observes a rapid decline, marking the senescence period. In contrast, SA's growth phase lasts longer (Fig. 2 b2), spanning five months, beginning gradually in April, accelerating until July, and peaking in September. However, after reaching its peak, SA swiftly enters the senescence phase.

Feature indices

Wetlands in YRD were primarily classified into three main types: salt marsh vegetation, tidal flat, and water body, with a further subdivision of PA and SA within the salt marsh vegetation. To facilitate precise monitoring, we incorporated five commonly used remote sensing indices: NDVI, EVI, Normalized Difference Water Index (MDWI), Modified Normalized Difference Water Index (mNDWI), and Land Surface Water Index (LSWI) (Eq. 1–5). Specifically, NDVI and EVI were employed for vegetation detection, MDWI and mNDWI for surface water detection, and LSWI as an auxiliary index for identifying green vegetation (Li et al. 2022a, b; Zeng et al. 2022). In addition, we referred to monitoring algorithms developed in recent studies (Wang et al. 2021b) specifically for extracting coastal vegetation (Cveg) and coastal water bodies (Cwat) (Eq. 6 and 7).

$$NDVI = \frac{\rho_{nir} - \rho_{red}}{\rho_{nir} + \rho_{red}} \tag{1}$$

$$EVI = 2.5 \times \frac{\rho_{nir} - \rho_{red}}{\rho_{nir} + 6 \times \rho_{red} - 7.5 \times \rho_{blue} + 1} \tag{2}$$

$$NDWI = \frac{\rho_{green} - \rho_{nir}}{\rho_{green} + \rho_{nir}} \tag{3}$$

$$mNDWI = \frac{\rho_{green} - \rho_{swir1}}{\rho_{green} + \rho_{swir1}} \quad (4)$$

$$LSWI = \frac{\rho_{nir} - \rho_{swir1}}{\rho_{nir} + \rho_{swir1}} \quad (5)$$

$$Cveg = (EVI \geq 0.1) and (NDVI \geq 0.2) and (LSWI > 0) \quad (6)$$

$$Cwat = (mNDWI > EVI or NDWI > EVI) and (EVI < 0.1) \quad (7)$$

where $\rho_{blue}, \rho_{green}, \rho_{red}, \rho_{nir}, and \rho_{swir1}$ are the surface reflectance values of blue, green, red, near-infrared, and shortwave infrared1 bands in Landsat 5/7/8 and Sentinel-2 images.

Supervisory classification and accuracy assessment

Random Forests (RF) model is a widely employed machine learning method for supervisory classification in remote sensing applications (Watts et al. 2009; Stumpf and Kerle 2011; Belgiu and Drăguţ, 2016; Chen et al. 2022), which combines the strength of decision trees with random subsampling and feature selection. However, the model has exhibited relatively low sensitivity to overfitting, while displaying higher sensitivity to the selection of sampling points (Rodriguez-Galiano et al. 2012; Belgiu and Drăguţ, 2016). Given the significant inter-annual variability in the YRD wetland, the identification of reliable sample points that span across different years is a challenge. Therefore, we selected new samples from the imagery nearly every year, with a total of 4391 samples throughout the time series (Fig. 2c).

The whole supervisory classification process can be divided into the following steps: (1) adding sample points through the optimal phase remote sensing images by referring to the interpretation signs in Fig. 1 c1–c4, (2) following the image processing approach used for phenology extraction, we synthesized remote sensing images for each of the three periods and inputting the feature indices bands for supervised classification, (3) obtained the preliminary annual supervised classification maps as a result. Due to the significant striping artifacts in the ETM + imagery in 2011, the mapping results were subject to considerable errors; therefore, (4) for the year 2011, we only selected the imagery from the less-affected period of 6 to 10 months for training and (5) manually corrected erroneous patches based on field surveys and visual interpretation, including oilfield, cultivated land, aquaculture, salt pan, and delineated ponds from the water body within the terrestrial interior of the wetland (Fig. 1 c1). (6) For estimating how well the resulting RF model performed, we used 70% of the samples to train the trees with the remaining 30% used in an internal cross-validation technique, then generated a confusion matrix and calculated the kappa coefficient and accuracy.

Statistical analysis

Landscape indices

Landscape indices are quantitative measures used to assess and describe the spatial arrangement and composition of landscapes (Tischendorf 2001). These indices provide valuable insights into the structure, connectivity, fragmentation, and heterogeneity of landscapes, providing a deeper understanding of landscape dynamics and ecological processes (Li and Wu 2004). Here, we selected nine landscape pattern indices (Table 1) to quantitatively describe the landscape pattern of the YRD wetland in five dimensions: area, landscape fragmentation, shape, diversity and aggregation. Then, we calculated the landscape pattern indices of the YRD wetland from 1986 to 2022 using Fragstats 4.2.1 software.

Regression analysis

We calculated the inter-annual variation and trends in YRD wetland area for the period 1986–2022 through piecewise linear regression models with a test at the 5% significance level.

To assess the impact of long-term hydrological processes on wetland areas, we employed a stepwise multiple linear regression model. This model necessitates comprehensive diagnostic evaluations, encompassing three key aspects: collinearity, significance, and the Durbin-Watson (DW) test. Collinearity indicates a high correlation among independent variables, with a Variance Inflation Factor (VIF) exceeding 10 signifying strong collinearity. Significance assessment relies on the P-value for regression coefficients, with P-values below 0.05 allowing rejection of the null hypothesis. Lastly, the DW test detects temporal

Table 1 Landscape indices, dimensions and meanings

Dimensions	Landscape indices	Meanings
Area	Largest patch index (LPI)	Percentage of the largest patch of a landscape
Fragmentation	Interspersion and juxtaposition Index (IJI)	Arrangement and interspersion of landscape
	Splitting index (SPLIT)	Splitting or fragmentation of patches
	Patch density (PD)	number of patches per unit area in a landscape
Shape	Landscape shape index (LSI)	The complexity of patch shapes in a landscape
	Perimeter-area fractal dimension (PAFRAC)	Irregularity and complexity of patch boundaries
Diversity	Shannon's evenness index (SHEI)	Evenness or uniformity of patch type
Aggregation	Aggregation index (AI)	spatial clustering or aggregation of landscape
	Contagion (CONTAG)	Reflects the connectivity of the landscape

correlation in regression model residuals, with critical values determined based on sample size (n) and the number of independent variables (k) using a table lookup method.

We established the potential relationships between sediment delivery (SE), runoff (RU), cumulative sediment delivery (SE+), cumulative runoff (RU+) and landscape indices to explore the factors driving landscape pattern evolution in the YRD wetland. Firstly, we examined the correlation between hydrological data and landscape indices, including the Pearson correlation coefficient and Spearman correlation coefficient. Secondly, based on the correlation coefficients, we established three distinct conditions for further analysis. Condition 1: using the Pearson correlation coefficient, we selected variables with $P < 0.001$ and conducted simple linear regression between the qualifying landscape pattern indices and the hydrological variables that exhibited a significant influence. Condition 2: for landscape indices that did not meet Condition 1, we used the Spearman correlation coefficient and selected two hydrological variables that simultaneously satisfied $P < 0.001$ or $P < 0.01$, then performed either multivariate nonlinear fitting or segmented linear fitting. Condition 3: if none of the conditions were met, we exclusively plotted scatter plots of the hydrological variables that demonstrated higher correlation coefficients. Through these systematic steps, our goal was to investigate the relationships between each landscape index and hydrological forces.

Results

Spatial changes of YRD wetland during 1986–2022

A total of 37 spatial distribution maps depicting the typical salt marsh vegetation in the YRD wetland for the period 1986–2022 were generated. The overall classification accuracy exceeded 96%, with a minimum Kappa coefficient value of 0.94, indicating that our classification results are reliable and highly accurate (Fig. 2c). Over the course of these 37 years, we present eight maps that are representative (Fig. 3). It is evident that in the past four decades, the YRD wetland has undergone substantial changes in terms of morphology, riverine pathways, and typical salt marsh vegetation.

In the early stages of the formation of the YRD, 1986, the wetland exhibited a relatively regular and open elliptical shape, with the typical salt marsh vegetation, PA, primarily distributed along the inland tidal flats on both sides of the Yellow River. Subsequently, as river erosion intensified, by 1990, the shape of the wetland became increasingly pointed, resembling a bird's beak.

Later, in 1996, a notable year for the YRD wetland, the long-established southeastward outlet channel was abandoned artificially, giving way to a new northeastward channel. Initially, the new channel had a smaller mouth, but by 2006, after nearly 10 years of development, the northeastward channel gradually expanded and formed one of the two major branches of the YRD wetland, alongside the southeastward channel. Furthermore, in 2006, extensive seasonal water ponds started to emerge in the southern part of the YRD wetland.
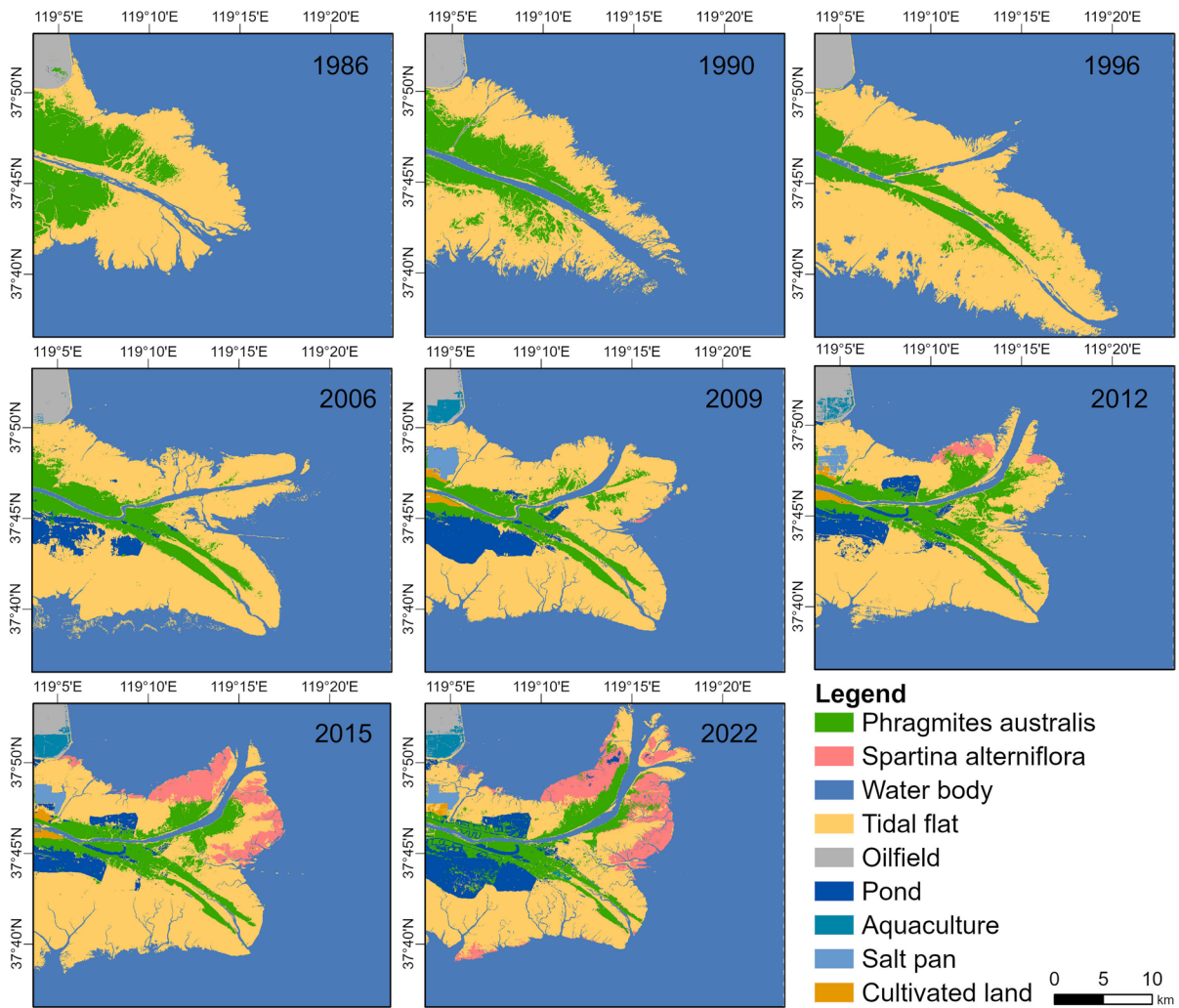
Fig. 3 Eight representative spatial maps of the saltmarshes in the YRD wetland were selected from 1986 to 2022

In 2009, fragmented patches of SA began to be observed, particularly in areas close to the coastal tidal flat. Additionally, human footprints such as aquaculture ponds, cultivated land, and salt fields gradually became evident in the same year. By 2012, the northeastern branch of the new flow path had further extended towards the ocean. Near the coastal areas, apparent patches of SA were observed, indicating its successful colonization. Simultaneously, larger seasonal water ponds also appeared in the northern part of the YRD wetland.

Over the subsequent decade, the SA flourished and expanded its coverage, progressively extending its territory from the coastal tidal flats towards the inland

areas and becoming another dominant species in this ecosystem. Furthermore, by 2022, it gradually started to encroach on the habitat of the established dominant species in the region, PA, which traditionally thrived along the Yellow River. Moreover, the morphological transformation of the YRD wetland during this period witnessed the continuous strengthening of the northeastern flow path, while the southeastern flow path gradually declined.

Patch area changes of YRD wetland during 1986–2022

Through visualizing the temporal changes of patches area in the YRD wetland over the past 37 years, we identified three stages of landscape pattern evolution: rapid expansion stage, gradual decline stage, and bio-invasion stage (Fig. 4a). From 1986 to 1997 was the first stage of wetland expansion. During these 12 years, both total wetland area (sum of the PA, SA,
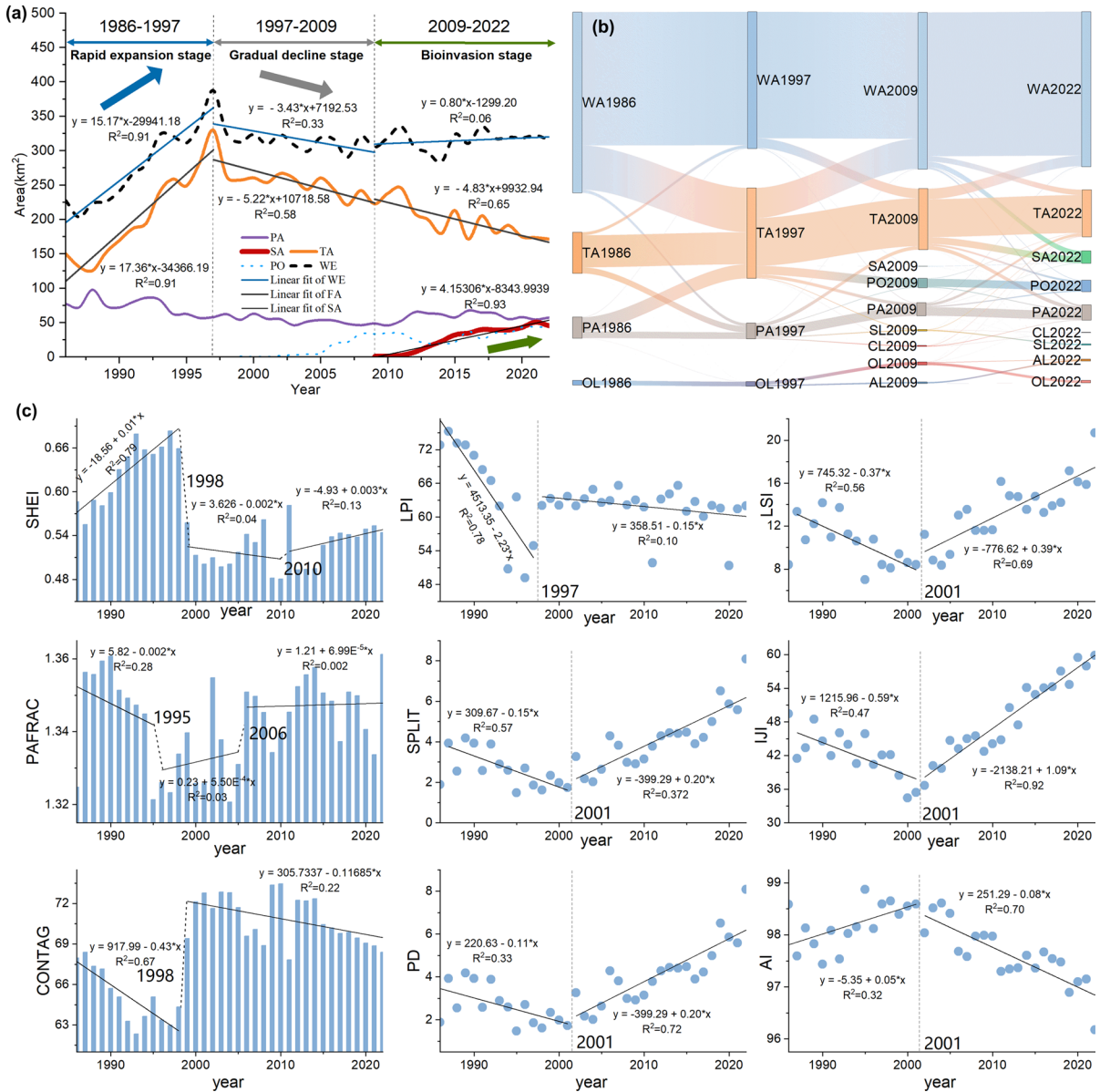

Fig. 4 Three phases of the wetland landscape evolution in the YRD wetland during 1986–2022. (**a**) Temporal variation curve and piecewise linear fitting line of wetland typical patch area from 1986 to 2022. (**b**) Sankey map of wetland patch transfer at four key time nodes (1986, 1997, 2009, 2022). (**c**) Inter-annual variation and piecewise linear trend fitting of wetland landscape indices in the YRD wetland from 1986 to 2022.

PA, SA, TA, PO, and WE represent the areas of *Phragmites australis*, *Spartina alterniflora*, tidal flat, pond, and wetland, respectively. The wetland area is the sum of the SA, PA, PO, and TA areas. WA, SL, CL, OL and AL represent the areas of water body, salt pan, cultivated land, oilfield, and aquaculture, respectively

tidal flat, and pond area) and tidal flat area showed a rapid increasing trend, with a 70% increase in the wetland area, reaching the peak of the entire time series in 1997 at 387.62 km^2, which laid the foundation for the wetland pattern. During this period, however, the dominant salt marsh vegetation, PA, was reduced by 25%. The second stage is the wetland decline stage, from 1997 to 2009, during which the wetland and tidal flat areas showed a slow declining trend, with the area of wetland reduced by 21% and PA reduced by 16%. The third stage is the bio-invasion stage. From 2009 to 2022, SA demonstrated a trend of rapid increase, with an area increase of 68 times relative to 2009, expanding at an average rate of 3.44 km^2 per year, approaching the area of PA by 2021 and becoming another dominant species in the YRD wetland. During the same time period, the PA area increased by 18%, however, extensive tidal flat areas were being encroached upon by SA, resulting in the tidal flat area being reduced by 23%.

Making a general observation of the transition matrix of patch areas across the three stages (Fig. 4b), we can draw four findings: (1) the YRD wetland underwent three different strengths of patch changes; (2) in the first stage, although there were significant variations in patch flows, the types of changes were relatively simple; (3) in the second stage, there was a noticeable increase in human activities, leading to an increase in the transfer flows and the density of the flow network; (4) In the third stage, although the area size of the transition between patches decreased, the network formed by the change flows became more complex.

In the first stage, the area of tidal flats doubled in size, with 161.77 km^2 contributed by wetland, of which 51.57 km^2 was contributed by PA, indicating a certain degree of degradation in the PA ecosystem. In the second stage, an area of 35.19 km^2 of tidal flat transformed into waterbody, signifying increased seawater intrusion. Additionally, a small portion of the tidal flat was converted into pond, salt pan, and cultivated land, indicating the manifestation of human activities. In the third stage, an area of 24.79 km^2 of tidal flat and 19.27 km^2 of water body were encroached upon by SA, while 38.38 km^2 of tidal flat was occupied by water body. Furthermore, an area of 19.55 km^2 of the water body transformed into a tidal flat, accounting for the counterbalance of both erosion and deposition in the tidal flat during this stage.

Compared to wetland patch areas, the landscape indices can comprehensively reflect information about landscape composition and spatial configuration, representing a highly condensed characterization of landscape pattern features. The temporal variations of landscape indices from 1986 to 2022 displayed a dual-stage or tri-stage pattern, with notable differences observed in the timing and trends of various indices (Fig. 4c). LSI, SPLIT, LJI, and PD, which represent landscape shape complexity, fragmentation, interspersion and juxtaposition, and patch density, respectively, exhibited two distinct stages with the year 2001 serving as the turning point. From 1986 to 2001, these indices displayed a decreasing trend. However, after 2001, they exhibited a significant upward trend. Before 2001, the wetland tended to exhibit a trend towards regularity and uniformity, while afterwards, it became increasingly fragmented with more complex shapes. AI reflects the connectivity between each patch type, which, in contrast, exhibited a trend of initial increase followed by a decrease, with the year 2001 as a turning point.

LPI, representing the proportion of the largest patch in the wetland, showed a decreasing trend from 1986 to 1997 and remained relatively high thereafter (Fig. 4c). In the YRD, the largest patch was the water body, which was replaced by the tidal flat during the wetland expansion stage. Subsequently, as the tidal flat gradually receded, the water body area increased. Therefore, LPI is consistent with the changing trend of water body.

SHEI exhibited a significant increasing trend before 1988 (Fig. 4c). A higher value of the index indicates a closer proportion of different patch types and a higher level of evenness. This suggests that the evenness of the landscape continuously increased until 1998, after which it dropped significantly and remained at a low level. PAFRAC, reflecting the complexity of patch boundaries, gradually decreased before 1995 but experienced a sudden increase after 2006, maintaining a high level thereafter. Unlike AI, CONTAG reflects the overall connectivity of the landscape. Before 1998, the wetland exhibited poor connectivity with a declining trend. However, after 1998, the connectivity suddenly increased and then gradually declined at that higher level.

Hydrological forces of wetland patch area

Stepwise linear regression results (Table 2) indicate that the dependent variables of wetland, tidal flat, and PA passed the model diagnostics ($P_i < 0.001$; at the significance level of 0.05, n = 36 and k = 3, $1.35 < DW < 1.59$), and SE + and RU + passed the collinearity diagnostics ($VIF_{3-4} < 10$). The areas of wetland, tidal flat, and PA in the YRD wetland were significantly influenced by SE + and RU +, explaining 61.5%, 75.7% and 63.8% of their variations respectively, while RU and SE are excluded from the model. Specifically, the wetland and tidal flat area are positively correlated with the SE + ($\beta_{31} = 2.61$, $\beta_{32} = 4.62$), while the RU + shows a weak negative effect ($\beta_{41} = -0.023$, $\beta_{42} = -0.063$). However, for PA, as a hydrophilic vegetation, the situation is the opposite, as the RU + has a positive effect on its area ($\beta_{43} = 0.008$). SA is likely limited by sample size, with high VIF and overfitting indicated by adjusted R^2, concluding that the model fails. Therefore, we separately analyzed the relationship between SA and hydrological factors. There was a significant positive correlation between SA and RU + and SE + (Fig. 5b $P < 0.001$), and the linearly fitted models perform well (Fig. 5c).

Although the correlation between RU, SE and the important wetland patch areas (wetland, tidal flat, SA, and PA) were not statistically significant, we found an interesting phenomenon: in 1997, when the area of wetland and tidal flat reached the peak in the rapid expansion stage, the Yellow River experienced the most serious flow cutoff (lasted about 226 days), and both RU and SE showed a decreasing trend during the period of wetland expansion (Fig. 5 a1). This suggests that the formation and evolution of wetland area is not determined by the short-term effects of runoff and sediment delivery in the current year, but may instead be affected by processes and influences on longer time scales.

Hydrological forces of landscape pattern

The correlation of RU + and SE + with the landscape indices demonstrated a higher overall significance compared to RU and SE (Fig. 6 a1–a2). The indices that satisfied Condition 1 (in the Pearson correlation analysis of landscape indices and hydrological variables, $P < 0.001$) included PD, LSI, CONTAG, IJI, SPLIT, and AI, while LPI and SHEI satisfied Condition 2 (fail to meet the condition 1, but the significance of Spearman correlation analysis is $P < 0.001$ or $P < 0.01$), and PAFRAC satisfied Condition 3 (neither condition 1 nor condition 2 is satisfied).

The patch density (PD) in the YRD wetland increases with an increase in RU (Pearson's r = 0.65) and RU + (Pearson's r = 0.68) (Fig. 6 b1). The two fitted curves of the landscape pattern index (LPI) are shown in Fig. 6 b2. As RU + and SE + (both Spearman's r = − 0.51) increase, the maximum patch, that is the water body, continues to decline, indicating an increase in the total terrestrial wetland area. In other words, increasing RU + and SE + are associated with the expansion of YRD wetland, with both variables explaining 46% of the variation in LPI. The shape complexity, represented by the landscape shape index (LSI), significantly increases with increasing RU (Pearson's r = 0.57) and RU + (Pearson's r = 0.63) (Fig. 6 b3).

Among all the landscape indices, PAFRAC is the only index that is not sensitive to any of the hydrological variables. As shown in the Fig. 6 b4, most of the points are concentrated in the upper left quadrant, indicating a positive correlation with SE and RU, but

Table 2 Stepwise multiple linear regression results of YRD wetland patch area with hydrological variables

Patch area ($X_{i,\ i=1,2,3,4}$)	Adjusted R_i^2	DW_i	F_i	Constant β_{0i}	RU β_{1i}	VIF_1	SE + β_{3i}	VIF_3	RU + β_{4i}	VIF_4
Wetland	0.615	1.463	28.944	223.984***			2.611***	7.367	− 0.023***	7.367
Tidal flat	0.757	1.516	55.488	141.277***			4.620***	7.367	− 0.063***	7.367
PA	0.638	1.374	31.788	87.259***			− 0.868***	7.367	0.008***	7.367
SA	0.989	2.262	282.100	235.371**	− .025*	3.898	− 6.738***	141.503	0.066***	119.275

RU, SE +, RU + respectively represent runoff, cumulative runoff, and cumulative sediment delivery.

* means P ≤ 0.05, ** means p ≤ 0.01, and *** means P ≤ 0.001 (the same as below)
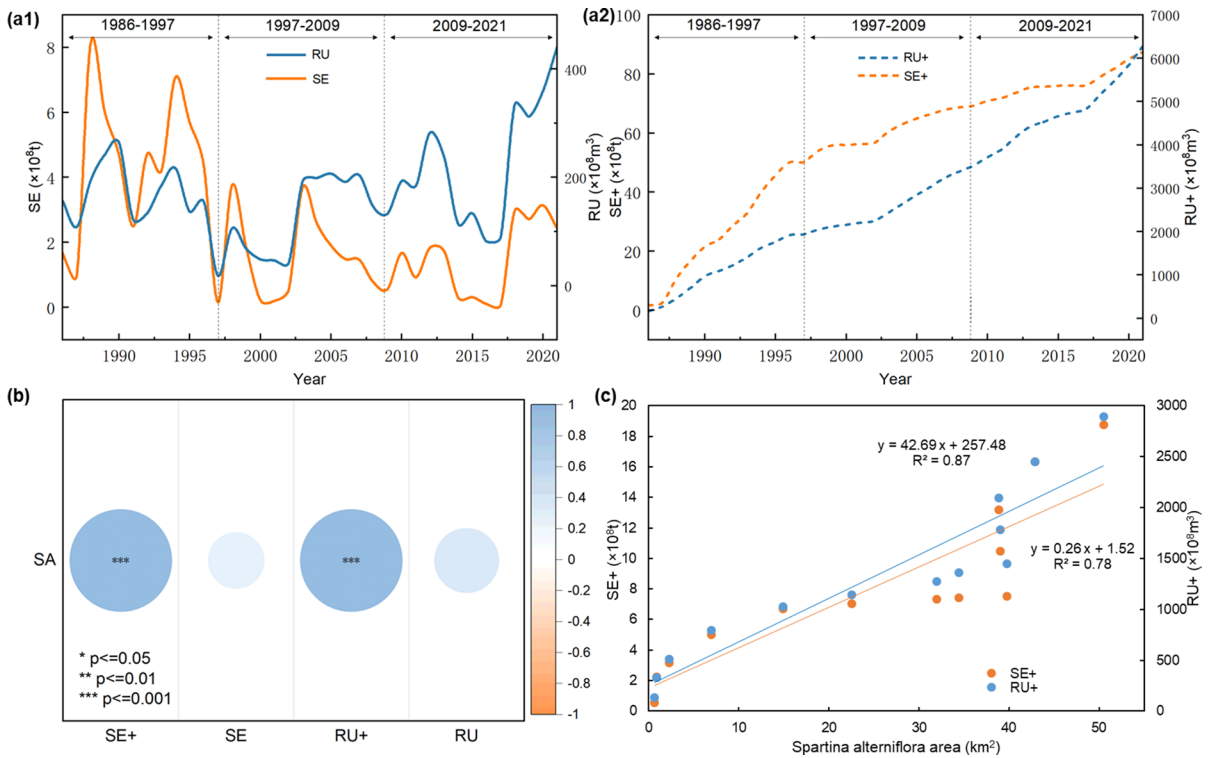
Fig. 5 The trends of annual runoff and sediment delivery (**a1**) and cumulative runoff and sediment delivery (**a2**) in Lijin hydrology station of the Yellow River from 1986 to 2021, and the Pearson correlation analysis (**b**) and linear fitting of SA area (**c**) with hydrological factors. SA, RU, SE, SE+, RU+ represent *Spartina alterniflora*, runoff, sediment delivery, cumulative runoff, and cumulative sediment delivery, respectively

without any statistical significance. CONTAG, which reflects landscape connectivity, decreases with SE (Fig. 6 b5, Pearson's r = − 0.55) but increases with the SE+ (Pearson's r = 0.53). RU (Pearson's r = 0.61) and RU+ (Pearson's r = 0.68) have a significant promoting effect on IJI (Fig. 6 b6), with explanatory values of 37% and 47%, respectively. This suggests that increased runoff intensifies the fragmentation of wetland patches.

SPLIT is significantly positively influenced by both RU+ (Pearson's r = 0.53) and SE+ (Pearson's r = 0.58) (Fig. 6 b7). SHEI is a special landscape index that reflects landscape uniformity. The results indicate that when RU+ at the Lijin station is less than 2040.63×10^8 m^3 and SE+ is less than 53.94×10^8 t, SHEI increases significantly with RU+ and SE+ (Fig. 6 b8), with explanatory values of 82% and 79%, respectively. However, beyond these values, the scatter plot becomes disordered and remains at a lower level. AI, which reflects landscape

spatial aggregation, decreases with RU (Pearson's r = − 0.58) and RU+ (Pearson's r = − 0.61) (Fig. 6 b9).

Discussions

Spatial changes

The shape of river delta is usually influenced by rivers, tides, and waves (Nienhuis et al. 2020). Though there was a sharp decrease in sediment delivery during the period 1986–1997 in the Yellow River (Wang et al. 2016), it is generally recognized that the morphology of YRD was river-dominated, given the reputation of the Yellow River for significant sediment delivery. However, there were differences in the drivers that dominated delta morphology in different stages. Firstly, before 1996, the morphology of the YRD exhibited a single lobe extending continuously
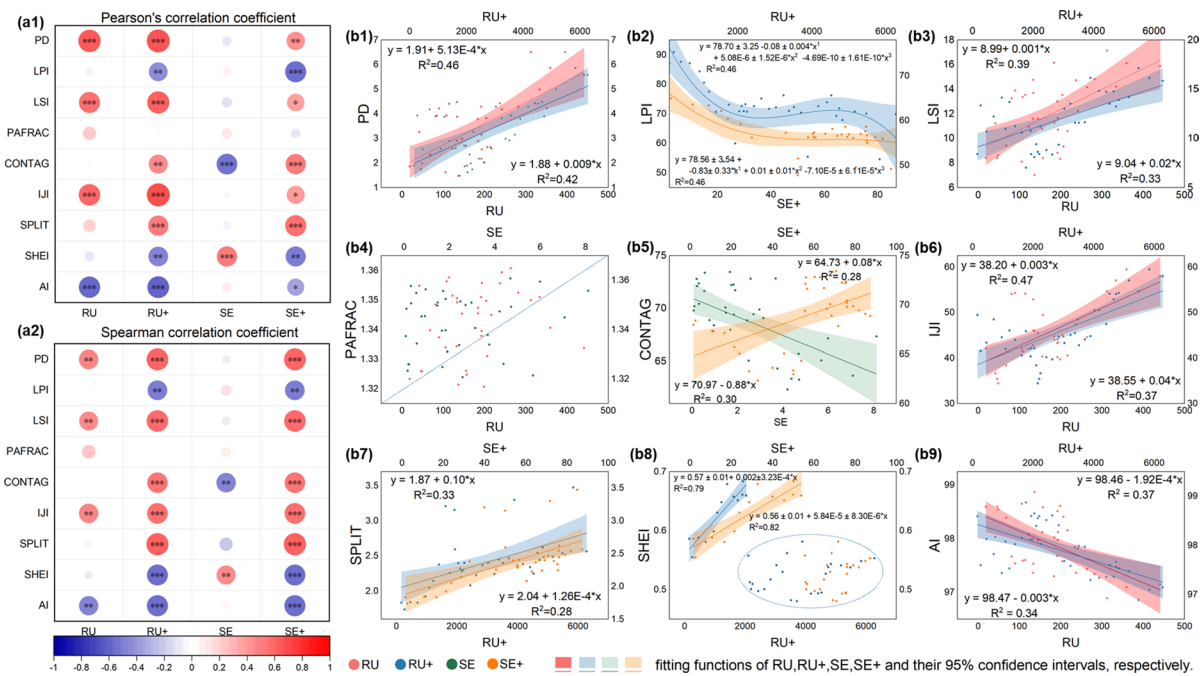
Fig. 6 Pearson and Spearman correlation coefficient matrix of landscape indices with hydrological drivers (a1-a2), and function fitting and scatter plots between them (b1-b9). Where, * means P≤0.05, ** means p≤0.01, and *** means P≤0.001. RU, RU+, SE, and SE+respectively represent the runoff, cumulative runoff, sediment delivery and cumulative sediment delivery of the Lijin hydrographic station. The fitting function and R^2 of the landscape index with a specific hydrological variable are displayed at the intersection of the two axes (except for SHEI, its fitting functions are displayed near the fitting trend lines)

towards the ocean, suggesting that the dominant factor was the river at this stage. Secondly, in 1996, the significant alteration that shaped the geomorphological structure of the estuary was driven by artificial diversion (Yu et al. 2021). This diversion was constructed to form land through sediment deposition at the Shengli oil field, which is on the near-sea area of the YRD.

After 1996, the newly formed northeast passage experienced continuous sediment deposition and continued extension to the ocean, while the abandoned estuary in the southeast weakened under marine erosion. Therefore, though the river discharge continued to play a dominant role, the erosive effects of ocean waves cannot be ignored in this stage. In sum, throughout the entire time series, the morphological changes in the YRD were predominantly governed by the influential force of the river, with marine erosion as the auxiliary factor, and human activities played a key role in the transformative changes in 1996.

Patch area changes

From 1986 to 2022, the wetland area underwent rapid expansion, followed by a gradual decline, and then a slow increase (Fig. 7a). This trend is mainly influenced by SE+and RU+, with SE+playing a more significant role, positively affecting wetland area (Yu et al. 2021), while RU+has a weaker negative impact (Fig. 7b).

The tidal flat area exhibited a pattern of initial increase followed by continuous decrease (Fig. 7a). In the first stage, the tidal flat area increased with rising SE+. In the second stage, 35.19 km^2 of tidal flats transitioned to seawater, while a small portion converted to ponds, salt fields, and cultivated land, indicating a consistent decline due to seawater intrusion and human activities. In the third stage, 24.79 km^2 of tidal flats were invaded by SA and 18.83 km^2 were eroded by seawater. Consequently, invasive SA and seawater erosion were the primary causes of tidal flat reduction in the third stage. The reduction of tidal flat
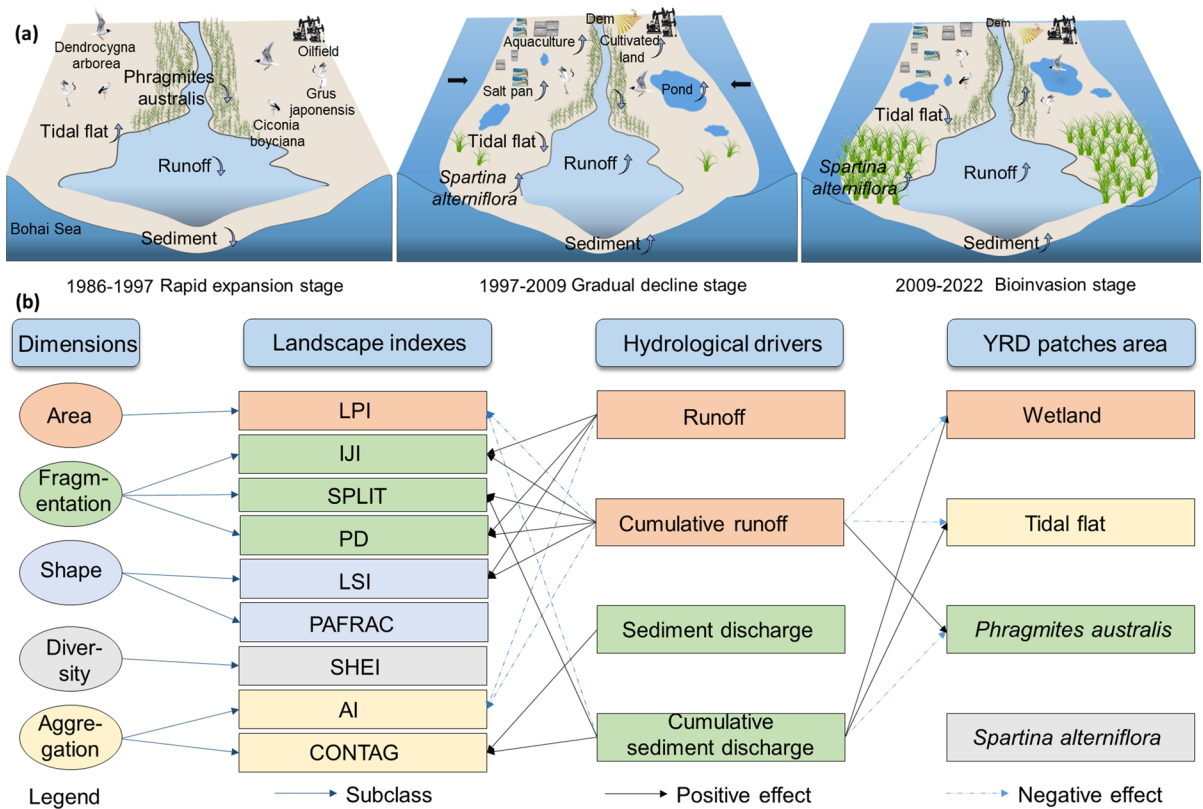
Fig. 7 Landscape pattern evolution diagrammatic drawing of YRD wetland (**a**), and hydrological driving factors of wetland landscape pattern evolution (**b**). The arrows in the diagrammatic drawing (**a**) represent the trend of the typical patch area during this period

area may lead to a series of ecological problems, such as reducing the habitat of rare and endangered birds, because more than 90% of water birds are dependent on the natural habitats like tidal flats (Li et al. 2013).

The PA area continuously decreased in the first and second stages but showed a slight rebound in the third stage (Fig. 7a). This was mainly influenced by RU + and SE +, where RU + played a positive role (Zhang et al. 2022) and SE + had a negative effect (Fig. 7b). Furthermore, the rebound in the third stage might also be attributed to recent ecological conservation policies. For instance, since 2008, the Yellow River Commission has been conducting regular freshwater replenishment to the YRD by ditching, promoting the recovery of the PA ecosystem.

For SA, in 2009, small patches were first observed in the YRD wetland. Around 2010, it rapidly expanded, which was positively associated with RU + and SE +. Moreover, research had revealed that the density, height and basal diameter of clonal ramets or sexual seedlings of SA increased with tidal inundation (Ma et al. 2019). Once the harm that SA caused was recognized, local control measures such as "enclosure and flooding" and "cutting and ploughing" were implemented, so that in 2022 we observed a decline of SA area.

Landscape pattern changes

The YRD wetland landscape fragmentation, shape complexity and aggregation were primarily

influenced by RU and RU + (Fig. 7b). It implies that under the erosive forces of flowing water, estuarine wetland landscapes tend to exhibit fragmentation and increasing complexity in shape, resulting in a decrease in landscape aggregation, particularly during flood events (Liu et al. 2022).

The YRD wetland landscape connectivity was mainly influenced by SE and SE +, which had a positive impact. SE played a significant role in shaping the connectivity of the YRD wetland (Fig. 7b). As sediment erodes and is transported by flowing water, it can contribute to the formation of channels, channel networks, and water pathways, enhancing the connectivity between different wetland areas. This promotes the exchange of water, nutrients, and biota within the wetland ecosystem, supporting the overall ecological health and functioning of the YRD wetland.

The hydrological driving effect on YRD patch evenness was controlled within a certain range: when the Lijin Station's cumulative runoff was lower than 2040×10^8 m^3 and cumulative sediment delivery was lower than 54×10^8 t, the Shannon's Evenness Index (SHEI) significantly increased with the increase of RU + and SE + which highlights the importance of regulating hydrological factors to achieve optimal patch evenness in the YRD wetland.

In addition, trends in landscape fragmentation, shape complexity, and aggregation showed important turning points around 2001, which are likely related to the formal operation of the large-scale hydraulic project, Xiaolangdi Reservoir. As a major water diversion and sediment control project in the lower reaches of the Yellow River, the Xiaolangdi Reservoir regulates the runoff and sediment delivery downstream (Xia et al. 2016) and therefore is likely to be an important factor influencing the landscape pattern in the YRD. Moreover, other landscape indices, such as SHEI, PAFRAC, CONTAG, and LPI, all showed important turning points in 1995–1998, which may have been affected by the period of flow stoppage and river diversion in the Yellow River.

Sources of uncertainty

We generated high spatial and temporal resolution maps of typical salt marsh vegetation in the YRD wetland from 1986 to 2022 and analyzed its landscape pattern changes and hydrological driving factors, providing a quantitative basis for the scientific

management of wetlands. However, due to the rapid changes in the landscape pattern of the YRD wetland, it is almost necessary to replace the sample points in GEE every year to achieve long-term supervised classification, and this visual-based sampling process may introduce potential and unavoidable errors. Moreover, the landscape pattern of the YRD wetland may also be influenced by other anthropogenic factors on the landscape such as salt fields, cultivated land, and aquaculture ponds, which may also contribute to the recent increase in landscape fragmentation and shape complexity (Li et al. 2021).

Conclusions

By combining high-resolution remote sensing images, we generated a 30-m resolution, annual time-scale dataset of typical salt marsh vegetation in the YRD from 1986 to 2022 and discussed the hydrological driving factors of wetland landscape evolution. We identified that the YRD has experienced three stages of landscape pattern changes with 1997 and 2009 as turning points, including the rapid expansion stage, gradual decline stage, and bio-invasion stage. The proliferation of *Spartina alterniflora* in the YRD needs to be given sufficient attention, because it is approaching the *Phragmites australis* habitats and competing with it for resources, potentially affecting the development of the *Phragmites australis* ecosystem. Furthermore, in the most recent two decades, human impacts have encroached upon this natural wetland area intensively, with seawater intrusion also taking place at the same time, threatening the tidal flat area. Moreover, we found that the YRD wetland landscape tended to exhibit fragmentation and increasing shape complexity with the increase of runoff and cumulative runoff, resulting in a decrease in landscape aggregation, while sediment delivery and cumulative sediment delivery had a positive impact on wetland landscape connectivity. To prevent the degradation of tidal flat and *Phragmites australis* areas, measures such as regulating sediment delivery and runoff from upstream regions and implementing ecological replenishment should be taken. To control the extensive proliferation of *Spartina alterniflora*, intervention measures can be implemented during the seedling stage. These findings extended the theoretical basis of landscape regime shift for the

conservation, management, and sustainable development of the YRD wetland. Further exploring the relative influences of natural factors (such as climate change, sea-level rise, and seawater intrusion) and human factors (such as water conservancy projects, dam construction, expansion of cultivated land, and aquaculture) on the changes in salt marsh vegetation of estuarine wetlands is recommended in future research.

Author contributions MQ: Methodology, Software, Validation, Writing—Original Draft, Writing—Review & Editing, Visualization. YL: Resources, Writing—Review & Editing, Supervision, Funding acquisition. PC: Software, Writing—Review & Editing. NH: Formal analysis. SW: Writing—Review & Editing. BF: Supervision. XH: Language proofreading.

Data availability The datasets generated during and/or analysed during the current study are available from the corresponding author upon reasonable request.

Declarations

Competing interests The authors declare that they have no known competing financial interests or personal relationships that could have appeared to influence the work reported in this paper.

Ethical approval and consent to participate Not applicable.

Consent for publication Not applicable.

References

Barbier EB (2014) A global strategy for protecting vulnerable coastal populations. Science 345(6202):1250–1251.

Belgiu M, Drăguţ L (2016) Random forest in remote sensing: a review of applications and future directions. ISPRS J Photogramm Remote Sens 114:24–31.

Bolton DK, Friedl MA (2013) Forecasting crop yield using remotely sensed vegetation indices and crop phenology metrics. Agric for Meteorol 173:74–84.

Chang D, Wang Z, Ning X, Li Z, Zhang L, Liu X (2022) Vegetation changes in Yellow River Delta wetlands from 2018 to 2020 using PIE-Engine and short time series Sentinel-2 images. Front Mar Sci 9:977050.

Chen A, Sui X, Wang D, Liao W, Ge H, Tao J (2016) Landscape and avifauna changes as an indicator of Yellow River Delta Wetland restoration. Ecol Eng 86:162–173.

Chen P, Wang S, Liu Y, Wang Y, Li Z, Wang Y, Zhang H, Zhang Y (2022) Spatio-temporal patterns of oasis dynamics in China's drylands between 1987 and 2017. Environ Res Lett 17(6):064044.

Chen, Y., & Kirwan, M. L. (2022). Climate-driven decoupling of wetland and upland biomass trends on the mid-Atlantic coast. *Nature Geoscience*, *15*(11), Article 11. https://doi.org/10.1038/s41561-022-01041-x

Cong P, Chen K, Qu L, Han J (2019) Dynamic changes in the wetland landscape pattern of the Yellow River Delta from 1976 to 2016 based on satellite data. Chin Geogra Sci 29(3):372–381.

Cox JR, Paauw M, Nienhuis JH, Dunn FE, van der Deijl E, Esposito C, Goichot M, Leuven JRFW, van Maren DS, Middelkoop H, Naffaa S, Rahman M, Schwarz C, Sieben E, Triyanti A, Yuill B (2022) A global synthesis of the effectiveness of sedimentation-enhancing strategies for river deltas and estuaries. Global Planet Change 214:103796.

Dong J, Xiao X, Menarguez MA, Zhang G, Qin Y, Thau D, Biradar C, Moore B (2016) Mapping paddy rice planting area in northeastern Asia with Landsat 8 images, phenology-based algorithm and Google Earth Engine. Remote Sens Environ 185:142–154.

Edmonds DA, Caldwell RL, Brondizio ES, Siani SMO (2020) Coastal flooding will disproportionately impact people on river deltas. Nat Commun 11:4741.

Edmonds DA, Toby SC, Siverd CG, Twilley R, Bentley SJ, Hagen S, Xu K (2023) Land loss due to human-altered sediment budget in the Mississippi River Delta. Nat Sustain. https://doi.org/10.1038/s41893-023-01081-0

Feng Y, Sun T, Zhu MS, Qi M, Yang W, Shao DD (2018) Salt marsh vegetation distribution patterns along groundwater table and salinity gradients in yellow river estuary under the influence of land reclamation. Ecol Ind 92:82–90.

Fu B, Meadows ME, Zhao W (2022) Geography in the Anthropocene: transforming our world for sustainable development. Geogr Sustain 3(1):1–6.

Goldberg L, Lagomasino D, Thomas N, Fatoyinbo T (2020) Global declines in human-driven mangrove loss. Glob Change Biol 26(10):5844–5855.

Gong B, Liu Z, Liu Y, Zhou S (2023) Understanding advances and challenges of urban water security and sustainability in China based on water footprint dynamics. Ecol Ind 150:110233.

Google Earth Engine (2023a). USGS Landsat 8 Level 2, Collection 2, Tier 1 | Earth Engine Data Catalog. https://developers.google.com/earth-engine/datasets/catalog/LANDSAT_LC08_C02_T1_L2/ Accessed 13 April 2023

Google Earth Engine (2023b). Sentinel-2 MSI: MultiSpectral Instrument, Level-2A | Earth Engine Data Catalog. https://developers.google.com/earth-engine/datasets/catalog/COPERNICUS_S2_SR/ Accessed 13 April 2023

Huang X, Duan Y, Tao Y, Wang X, Long H, Luo C, Lai Y (2022) Effects of Spartina alterniflora invasion on soil organic carbon storage in the beihai coastal wetlands of China. Front Mar Sci. https://doi.org/10.3389/fmars.2022.890811

Kong D, Miao C, Borthwick AGL, Duan Q, Liu H, Sun Q, Ye A, Di Z, Gong W (2015) Evolution of the Yellow River Delta and its relationship with runoff and sediment load from 1983 to 2011. J Hydrol 520:157–167.

Li S, Wang G, Deng W, Hu Y, Hu W-W (2009) Influence of hydrology process on wetland landscape pattern: A case study in the Yellow River Delta. Ecol Eng 35(12):1719–1726. https://doi.org/10.1016/j.ecoleng.2009.07.009

Li D, Chen S, Lloyd H, Zhu S, Shan K, Zhang Z (2013) The importance of artificial habitats to migratory waterbirds within a natural/artificial wetland mosaic, Yellow River Delta. China Bird Conserv Int 23(2):184–198.

Li Y, Dang B, Zhang Y, Du Z (2022b) Water body classification from high-resolution optical remote sensing imagery: achievements and perspectives. ISPRS J Photogramm Remote Sens 187:306–327.

Li G, Fang C, Qi W (2021) Different effects of human settlements changes on landscape fragmentation in China: evidence from grid cell. Ecol Ind 129:107927.

Li H, Wu J (2004) Use and misuse of landscape indices. Landscape Ecol 19(4):389–399.

Li S, Xie T, Bai J, Cui B (2022a) Degradation and ecological restoration of estuarine wetlands in China. Wetlands 42(7):90.

Li, L., Li, X., Niu, B., & Zhang, Z. (2023). A Study on the Dynamics of Landscape Patterns in the Yellow River Delta Region. Water, 15(4), Article 4. https://doi.org/10.3390/w15040819

Lin, Q., & Yu, S. (2018). Losses of natural coastal wetlands by land conversion and ecological degradation in the urbanizing Chinese coast. Scientific Reports, 8(1), Article 1. https://doi.org/10.1038/s41598-018-33406-x

Liu Y, Han J, Jiao J, Liu B, Ge W, Pan Q, Wang F (2022) Responses of flood peaks to land use and landscape patterns under extreme rainstorms in small catchments—a case study of the rainstorm of Typhoon Lekima in Shandong, China. Int Soil Water Conserva Res 10(2):228–239.

Liu C, Song C, Ye S, Cheng F, Zhang L, Li C (2023a) Estimate provincial-level effectiveness of the arable land requisition-compensation balance policy in mainland China in the last 20 years. Land Use Policy 131:106733.

Liu Y, Fu B, Wang S, Rhodes JR, Li Y, Zhao W, Li C, Zhou S, Wang C (2023b) Global assessment of nature's contributions to people. Science Bulletin 68(4):424–435.

Loucks DP (2019) Developed river deltas: are they sustainable? Environ Res Lett 14(11):113004.

Ma X, Yan J, Wang F, Qiu D, Jiang X, Liu Z, Sui H, Bai J, Cui B (2019) Trait and density responses of Spartina alterniflora to inundation in the Yellow River Delta, China. Mar Pollut Bull 146:857–864.

Montaño Y, Carbajal N (2008) Numerical experiments on the long-term morphodynamics of the Colorado River Delta. Ocean Dyn 58(1):19–29.

Murray NJ, Worthington TA, Bunting P, Duce S, Hagger V, Lovelock CE, Lucas R, Saunders MI, Sheaves M, Spalding M, Waltham NJ, Lyons MB (2022) High-resolution mapping of losses and gains of Earth's tidal wetlands. Science 376(6594):744–749.

Murray, N. J., Phinn, S. R., DeWitt, M., Ferrari, R., Johnston, R., Lyons, M. B., Clinton, N., Thau, D., & Fuller, R. A. (2019). The global distribution and trajectory of tidal flats. Nature, 565(7738), Article 7738. https://doi.org/10.1038/s41586-018-0805-8

Nienhuis, J. H., Ashton, A. D., Edmonds, D. A., Hoitink, A. J. F., Kettner, A. J., Rowland, J. C., & Törnqvist, T. E. (2020). Global-scale human impact on delta morphology has led to net land area gain. Nature, 577(7791), Article 7791. https://doi.org/10.1038/s41586-019-1905-9

Osland MJ, Chivoiu B, Enwright NM, Thorne KM, Guntenspergen GR, Grace JB, Dale LL, Brooks W, Herold N, Day JW, Sklar FH, Swarzenzki CM (2022) Migration and transformation of coastal wetlands in response to rising seas. Sci Adv 8(26):eabo5174.

Pang B, Xie T, Cui B, Wang Q, Ning Z, Liu Z, Chen C, Lu Y, Zhao X (2023) Adaptability of common coastal wetland plant populations to future sea level rise. Ecosyst Health Sustain 9:0005.

Paszkowski, A., Goodbred, S., Borgomeo, E., Khan, M. S. A., & Hall, J. W. (2021). Geomorphic change in the Ganges–Brahmaputra–Meghna delta. Nature Reviews Earth & Environment, 2(11), Article 11. https://doi.org/10.1038/s43017-021-00213-4

Reader, M. O., Eppinga, M. B., de Boer, H. J., Damm, A., Petchey, O. L., & Santos, M. J. (2022). The relationship between ecosystem services and human modification displays decoupling across global delta systems. Communications Earth & Environment, 3(1), Article 1. https://doi.org/10.1038/s43247-022-00431-8

Reid, W. V. (2005). Millennium Ecosystem Assessment: Ecosystems and Human Well-being. https://www.wri.org/research/millennium-ecosystem-assessment-ecosystems-and-human-well-being

Rodríguez, J. F., Saco, P. M., Sandi, S., Saintilan, N., & Riccardi, G. (2017). Potential increase in coastal wetland vulnerability to sea-level rise suggested by considering hydrodynamic attenuation effects. Nature Communications, 8(1), Article 1. https://doi.org/10.1038/ncomms16094

Rodriguez-Galiano VF, Ghimire B, Rogan J, Chica-Olmo M, Rigol-Sanchez JP (2012) An assessment of the effectiveness of a random forest classifier for land-cover classification. ISPRS J Photogramm Remote Sens 67:93–104.

Rosentreter, J. A., Laruelle, G. G., Bange, H. W., Bianchi, T. S., Busecke, J. J. M., Cai, W.-J., Eyre, B. D., Forbrich, I., Kwon, E. Y., Maavara, T., Moosdorf, N., Najjar, R. G., Sarma, V. V. S. S., Van Dam, B., & Regnier, P. (2023).

Coastal vegetation and estuaries are collectively a greenhouse gas sink. *Nature Climate Change*, *13*(6), Article 6. https://doi.org/10.1038/s41558-023-01682-9

Shammi SA, Meng Q (2021) Use time series NDVI and EVI to develop dynamic crop growth metrics for yield modeling. Ecol Ind 121:107124.

Song S, Wang S, Fu B, Liu Y, Wang K, Li Y, Wang Y (2020) Sediment transport under increasing anthropogenic stress: regime shifts within the yellow river. China Ambio 49(12):2015–2025.

Spencer T, Schuerch M, Nicholls RJ, Hinkel J, Lincke D, Vafeidis AT, Reef R, McFadden L, Brown S (2016) Global coastal wetland change under sea-level rise and related stresses: The DIVA Wetland Change Model. Global Planet Change 139:15–30.

Stumpf A, Kerle N (2011) Object-oriented mapping of landslides using random forests. Remote Sens Environ 115(10):2564–2577.

Sun C, Li J, Liu Y, Zhao S, Zheng J, Zhang S (2023) Tracking annual changes in the distribution and composition of saltmarsh vegetation on the Jiangsu coast of China using Landsat time series–based phenological parameters. Remote Sens Environ 284:113370.

Tischendorf L (2001) Can landscape indices predict ecological processes consistently? Landscape Ecol 16(3):235–254.

Törnqvist TE (2023) A river delta in transition. Nat Sustain. https://doi.org/10.1038/s41893-023-01104-w

Wan S, Qin P, Liu J, Zhou H (2009) The positive and negative effects of exotic Spartina alterniflora in China. Ecol Eng 35(4):444–452.

Wang X, Chen Y, Li Z, Fang G, Wang F, Liu H (2020) The impact of climate change and human activities on the Aral Sea Basin over the past 50 years. Atmos Res 245:105125.

Wang S, Fu B, Piao S, Lü Y, Ciais P, Feng X, Wang Y (2016) Reduced sediment transport in the Yellow River due to anthropogenic changes. Nat Geosci 9(1):38–41.

Wang X, Xiao X, Xu X, Zou Z, Chen B, Qin Y, Zhang X, Dong J, Liu D, Pan L, Li B (2021b) Rebound in China's coastal wetlands following conservation and restoration. Nature Sustainability 4(12):1076–1083.

Wang, X., Xiao, X., Xu, X., Zou, Z., Chen, B., Qin, Y., Zhang, X., Dong, J., Liu, D., Pan, L., & Li, B. (2021a). Rebound in China's coastal wetlands following conservation and restoration. *Nature Sustainability*, *4*(12), Article 12. https://doi.org/10.1038/s41893-021-00793-5

Wang H, Yang Z, Saito Y, Liu JP, Sun X, Wang Y (2007) Stepwise decreases of the Huanghe (Yellow River) sediment load (1950–2005): impacts of climate change and human activities. Global Planet Change 57(3):331–354.

Ward, N. D., Megonigal, J. P., Bond-Lamberty, B., Bailey, V. L., Butman, D., Canuel, E. A., Diefenderfer, H., Ganju, N. K., Goñi, M. A., Graham, E. B., Hopkinson, C. S., Khangaonkar, T., Langley, J. A., McDowell, N. G., Myers-Pigg, A. N., Neumann, R. B., Osburn, C. L., Price, R. M., Rowland, J., Windham-Myers, L. (2020). Representing the function and sensitivity of coastal interfaces in Earth system models. *Nature Communications*, *11*(1), Article 1. https://doi.org/10.1038/s41467-020-16236-2

Watts JD, Lawrence RL, Miller PR, Montagne C (2009) Monitoring of cropland practices for carbon sequestration purposes in north central Montana by Landsat remote sensing. Remote Sens Environ 113(9):1843–1852.

Xia X, Dong J, Wang M, Xie H, Xia N, Li H, Zhang X, Mou X, Wen J, Bao Y (2016) Effect of water-sediment regulation of the Xiaolangdi reservoir on the concentrations, characteristics, and fluxes of suspended sediment and organic carbon in the Yellow River. Sci Total Environ 571:487–497.

Xia H, Liu L, Bai J, Kong W, Lin K, Guo F (2020) Wetland ecosystem service dynamics in the yellow river estuary under natural and anthropogenic stress in the past 35 years. Wetlands 40(6):2741–2754.

Ye S, Song C, Shen S, Gao P, Cheng C, Cheng F, Wan C, Zhu D (2020) Spatial pattern of arable land-use intensity in China. Land Use Policy 99:104845.

Yin C, Pereira P, Zhao W, Barcelo D (2023) Natural climate solutions. The way forward. Geogr Sustain 4(2):179–182.

Yu D, Han G, Wang X, Zhang B, Eller F, Zhang J, Zhao M (2021) The impact of runoff flux and reclamation on the spatiotemporal evolution of the Yellow River estuarine wetlands. Ocean Coast Manag 212:105804.

Zeng, Y., Hao, D., Huete, A., Dechant, B., Berry, J., Chen, J. M., Joiner, J., Frankenberg, C., Bond-Lamberty, B., Ryu, Y., Xiao, J., Asrar, G. R., & Chen, M. (2022). Optical vegetation indices for monitoring terrestrial ecosystems globally. *Nature Reviews Earth & Environment*, *3*(7), Article 7. https://doi.org/10.1038/s43017-022-00298-5

Zhan C, Wang Q, Cheng S, Zeng L, Yu J, Dong C, Yu X (2023) Investigating the evolution of landscape patterns in historical subdeltas and coastal wetlands in the Yellow River Delta over the last 30 years: a geo-informatics approach. Front Mar Sci. https://doi.org/10.3389/fmars.2023.1115720

Zhang C, Gong Z, Qiu H, Zhang Y, Zhou D (2021a) Mapping typical salt-marsh species in the Yellow River Delta wetland supported by temporal-spatial-spectral multidimensional features. Sci Total Environ 783:147061.

Zhang X, Wang G, Xue B, Zhang M, Tan Z (2021b) Dynamic landscapes and the driving forces in the Yellow River Delta wetland region in the past four decades. Sci Total Environ 787:147644.

Zhang Y, Wang X, Yan S, Zhu J, Liu D, Liao Z, Li C, Liu Q (2022) Influences of Phragmites australis density and groundwater level on soil water in semiarid wetland, North China: which is more influential? Ecohydrol Hydrobiol 22(1):85–95.

Zhang R, Tian D, Wang J, Niu S (2023) Critical role of multidimensional biodiversity in contributing to ecosystem sustainability under global change. Geogr Sustain 4(3):232–243.

Zhou K (2022) Wetland landscape pattern evolution and prediction in the Yellow River Delta. Appl Water Sci 12(8):190.